

Article

Influence Mechanism of a New-Style Resonator on Band Gap of Locally Resonant Phononic Crystal Double Panel Structure

Yujia Xiang ¹, Molin Chen ², Denghui Qian ² and Zhiyu Shi ^{1,*}

¹ State Key Laboratory of Mechanics and Control of Mechanical Structures, College of Aerospace Engineering, Nanjing University of Aeronautics and Astronautics, Nanjing 210016, China; yjxiang@nuaa.edu.cn

² School of Naval Architecture & Ocean Engineering, Jiangsu University of Science and Technology, Zhenjiang 212100, China; mlchen@just.edu.cn (M.C.); dhqian@just.edu.cn (D.Q.)

* Correspondence: zyshi@nuaa.edu.cn

Abstract: Based on the previous studies on the stubbed-on locally resonant phononic crystal (LRPC) double panel structure (DPS) made of a two-dimensional periodic array of a two-component cylindrical LR pillar connected between the upper and lower plates, the stubbed-on LRPC DPS with soft shell surrounded and simplified model with additional springs surrounded are proposed. According to the changes in structural form, the wider band gap is opened, and the novel formation mechanism of the band gap is revealed. Finite element method (FEM) is applied to calculate the band structures. Numerical results and further analysis demonstrate that the soft shell only affects the bands corresponding to symmetric vibration mode and makes the bands shift up. In addition, the influences of density and Poisson's ratio of soft shell on the band gap can be ignored, but the starting frequency keeps still, and band gap width increases first and then keeps constant with the increase of elasticity modulus. All the results provide a theoretical basis for the study of vibration and noise resistance in engineering.



Citation: Xiang, Y.; Chen, M.; Qian, D.; Shi, Z. Influence Mechanism of a New-Style Resonator on Band Gap of Locally Resonant Phononic Crystal Double Panel Structure. *Crystals* **2022**, *12*, 609. <https://doi.org/10.3390/cryst12050609>

Academic Editors: Bernard Bonello and Luis M. Garcia-Raffi

Received: 18 March 2022

Accepted: 23 April 2022

Published: 26 April 2022

Publisher's Note: MDPI stays neutral with regard to jurisdictional claims in published maps and institutional affiliations.



Copyright: © 2022 by the authors. Licensee MDPI, Basel, Switzerland. This article is an open access article distributed under the terms and conditions of the Creative Commons Attribution (CC BY) license (<https://creativecommons.org/licenses/by/4.0/>).

Keywords: locally resonant phononic crystal; double panel structure; soft shell; band structure; symmetric vibration mode

1. Introduction

Vibration and noise control is a vitally important problem in many engineering fields, such as submarines, aircraft, automobiles, architecture, large generator units, and so on [1–4], which illustrates that the theory of vibration and noise reduction has an extremely important position in the fields of national defense and civil use. Especially in recent decades, the problem of vibration and noise pollution has attracted more and more people's attention with the great progress made in industry and transportation, which promotes the academic and engineering circles that have been committed to researching and solving this kind of hot issue. Through extensive theoretical and experimental research on vibration and noise control techniques, traditional vibration, and noise reduction technology has developed into a complete system and tends to mature. Hence, the new control method is urgently needed to meet the needs of people for a more comfortable vibration and noise environment.

The propagation of vibration mostly takes a solid structure as the main medium, in which the propagation distance is long, and the attenuation is small and keeps on radiating noise outwards during the transmission process. Take the aircraft cabin as an example; the structural vibration induced by engine vibration and aerodynamics propagates along with the containment structure of the cabin and radiates noise to the cabin, which brings a certain influence on passengers' comfort. Consequently, vibration and noise control are usually carried out from the propagation path if the vibration source or noise source is given.

The containment structures of industrial products mostly adopt different DPSs with multifunctional properties such as lightweight, high rigidity, great load, and so on [5–7]. Take the typical airplane construction as an example; aircraft fuselage structure is generally a semi-hard-shell structure composed of a transverse frame, longitudinal truss, beam, and skin. In addition, the skin and inner decorative plate form a double-deck structure, and the transverse frame, longitudinal truss, beam, and so on divide the interlayer between the double plate structure into independent chambers. Therefore, researching the vibration control of DPS will play an active role in reducing vibration and noise in engineering.

In recent years, PC has attracted a lot of attention from researchers, which is a kind of artificial periodic composite material with an elastic band gap [8,9]. In the frequency range of band gap, vibration cannot be propagated along with PC, thus it has broad prospects in the field of vibration and noise control, which provides a new idea for restraining vibration and reducing noise generated by the structure. PC can be divided into Bragg scattering [8,10] and LR [9,11] PCs from the formation mechanisms of band gap. The significant difference between them is that only LRPC can apply appropriate size to control vibration propagation in the low-frequency region [9], which provides a new approach to reducing vibration and noise in the unmanageable low-frequency region of engineering.

Up to now, research on plates with the design idea of PC introduced was mostly concentrated on stubbed-on LRPC single plate, which is constructed by periodically attaching resonant units onto the surface of the base plate. Oudich et al. [12] studied the band gap properties of two-component and three-component stubbed-on PC single plates constructed by periodically attaching rubber stubs without and with Pb capped on the surface of the base plate, and results showed that the extremely low-frequency band gap was opened by the coupling between a localized mode in the stub and Lamb mode in the plate. The two-component and three-component double-side stubbed-on LRPC single plates were proposed and researched by Assouar et al. [13]. By comparing the corresponding band structures, the proposed double-sided structure gives a stronger coupling between the localized resonant modes and Lamb modes than one-sided structures, which leads to widening the band gap effectively. Hsu [14] proposed a two-dimensional PC composed of an array of stepped resonators on a thin slab. Research shows that the structure exhibits LR and Bragg scattering band gaps simultaneously, and the polarization states of incident slab modes influence the spectra of resonances, power transmission, and attenuation. Besides simplifying the resonator of stubbed-on structure to “spring-mass,” Xiao et al. [15] researched the propagation of flexural waves in an LR thin plate made of a two-dimensional periodic array of spring-mass resonators attached to a thin homogeneous plate. Results demonstrate that the resonant frequency of “spring-mass” has great relations with the band gap. According to the low-frequency mechanical vibration generated by the power systems on the ship, a single-phase spiral-shaped PC was designed and analyzed based on the locally resonant modes by Ruan et al. [16]. The vibration characteristics of the PC plates with different boundary conditions and loads were numerically simulated, and groups of experimental tests were conducted to verify the abilities of vibration isolation for three kinds of PCs.

In this paper, we investigated the propagation characteristics of flexural and longitudinal vibrations in a stubbed-on LRPC DPS consisting of a two-layer plate with periodically attached cylindrical LR pillars between the upper and lower plates in which the resonator is surrounded by a soft shell. Furthermore, the simplified model with additional springs surrounded is also proposed to help understand the effect of soft shell on the band gap. Different from the previous LRPC DPS, the soft shell and additional springs are added. According to the changes in structural form, the corresponding novel phenomenon and formation mechanism of band gap change are studied. Further, the elasticity modulus, Poisson’s ratio, and density are picked as the influencing parameters to investigate the effects of the soft shell material on the band gap. All the results are expected to be of theoretical significance in engineering application prospects in the field of vibration and noise control.

2. Model and Method

As shown schematically in Figure 1a, the model proposed in this paper was constructed by periodically depositing the 2-component cylindrical LR pillars squarely onto the surfaces of the upper and lower homogeneous LRPC plates. In addition, each resonator unit was surrounded by a soft shell, as shown in Figure 1b. In a unit cell, the material of the first and last layers in the pillar was rubber; the materials of the plates and middle layer in the pillar were epoxy and Pb, respectively. The lattice constant, thickness of base plates, radius of pillar, height of rubber layer in the pillar, height of Pb layer in the pillar, outer radius of added soft shell, and inner radius of added soft shell was denoted by a , e , r , h_1 , h_2 , R_{S1} , and R_{S2} , respectively. The materials' parameters used in calculations are displayed in Table 1, and all the materials were assumed to be elastically isotropic. In addition, the density of the soft shell was assumed to be zero at first; that is the effect of density on band structure was studied on the basis of the research on the stiffness of the soft shell. The elasticity modulus E_a and Poisson's ratio μ_a of soft shell are presupposed to be $1.175 \times 10^5 \text{ N/m}^2$ and 0.469, respectively.

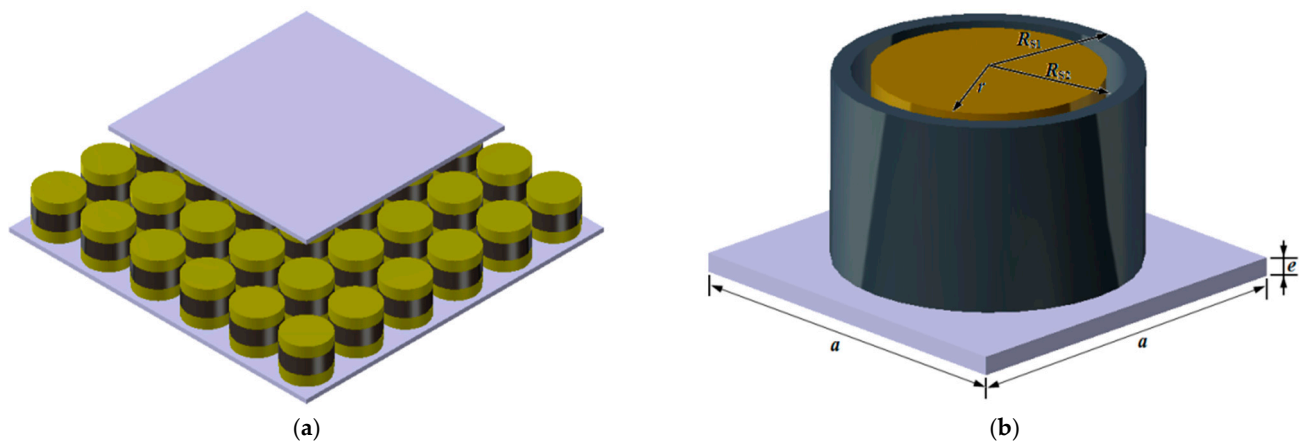


Figure 1. (a) The stubbed-on LRPC DPS with resonator unit surrounded by soft shell (soft shell is ignored), and (b) its unit cell (upper plate is ignored), a is the lattice constant, e is the thickness of base plates, r is the radius of pillar, R_{S1} is the outer radius of added soft shell and R_{S2} is the inner radius of added soft shell.

Table 1. Materials' parameters used in calculations in Figure 2.

Material	Mass Density (kg/m ³)	Young's Modulus (10 ¹⁰ N/m ²)	Poisson's Ratio
Epoxy	1180	0.435	0.368
Rubber	1300	1.175×10^{-5}	0.469
Pb	11,600	4.08	0.37

The finite element method (FEM) was applied to calculate the band structure of the proposed DPS, and commercial software COMSOL Multiphysics was adopted to help implement this. On account of the infinitely periodicity of PC structure in the x - y plane, only the unit cell was needed to take into consideration, and the periodic boundary condition was applied to the interfaces between the nearest unit cells [12,17].

$$u_i(x + a, y + a) = u_i(x, y)e^{-i(k_x a + k_y a)}, \quad (i = x, y, z) \quad (1)$$

here, if i equals to x , y , and z , u_i represents the components of 3-dimensional displacement field u along x -direction, y -direction and z -direction, respectively. In addition, k_x and k_y are the components of the Bloch wave vector k limited in the irreducible first Brillouin zone (1BZ).

The stress-free boundary condition was applied to all the other surfaces except for the interfaces. In addition, the default tetrahedral mesh provided by the software was used during the meshing of the unit cell.

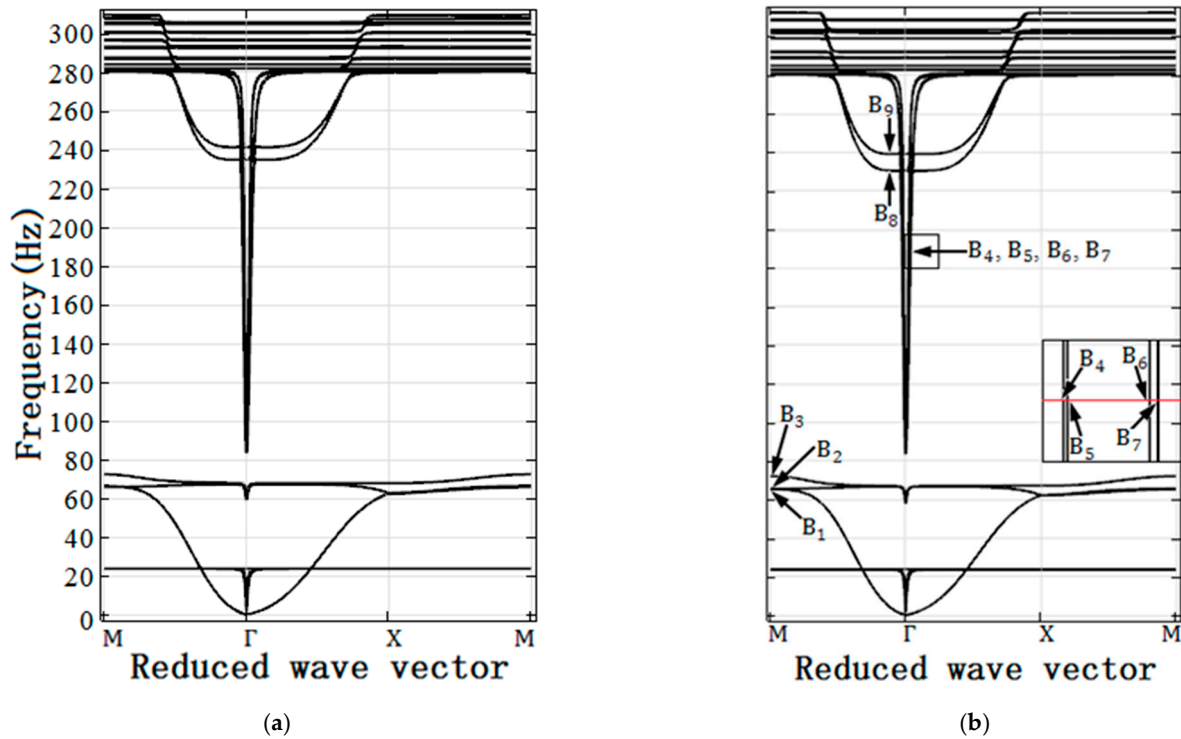


Figure 2. Band structures of stubbed-on LRPC DPSs (a) with and (b) without surrounded soft shell.

By substituting periodic boundary condition (Equation (1)) to free vibration characteristic equation of FEM, it gives:

$$(\mathbf{K} - \omega^2 \mathbf{M})\mathbf{u} = \mathbf{0} \quad (2)$$

here, what should be noted is that the elements in stiffness matrix \mathbf{K} and mass matrix \mathbf{M} are coupled with the items containing the Bloch wave vector k , such as $e^{-ik_x a}$, $e^{-ik_y a}$, $e^{-i(k_x a + k_y a)}$ and so on. They are not the original structural stiffness and mass matrices of the classical FEM anymore.

As shown in Equation (2), it is a typical generalized eigenvalue problem for ω^2 , which has been used to calculate band structures of different PC structures for several years [12–20]. A series of eigenfrequencies can be obtained by solving the equation for each given Bloch wave vector k . Finally, the band structure of LRPC DPS can be obtained by scanning all k in the irreducible first Brillouin zone (1BZ).

3. Numerical Results and Analyses

In Reference [18], the formation mechanisms and influence rules of band gap of the proposed stubbed-on LRPC DPS but without a soft shell surrounded were investigated in detail. Numerical results and further analysis demonstrated that a band gap with a low starting frequency and wide band width can be opened by the coupling between the dominant vibrations of stubbed-on pillars and plate modes if the excitation and response points are picked on different sides of the DPS. Then, the bands corresponding to symmetric and antisymmetric vibration modes are displayed exclusively in DPS. In addition, the influences of soft material viscosity and geometrical parameters such as pillar radius, plate thickness, and lattice constant on the band gap are studied and explained.

In this paper, the effect mechanisms and rules of surrounded soft shell on the band gap are studied emphatically and displayed below.

3.1. Band Structures of LRPC DPSs with and without Surrounded Soft Shell

Figure 2a shows the band structure of stubbed-on LRPC DPS with a resonator unit surrounded by soft shell. As a comparison, the band structure of LRPC DPS without a soft shell surrounded was also calculated, as shown in Figure 2b. All the materials' parameters and geometric parameters used in calculations are shown in Tables 1 and 2, respectively. By comparing Figure 2a,b, the added soft shell only has effect on the band corresponding to symmetric vibration mode B_8 , but hardly any effect on the bands corresponding to modes B_1 – B_7 and B_9 labeled in Figure 2b. Moreover, the band corresponding to B_8 is shifted upward by surrounding the soft shell.

Table 2. Geometric parameters used in calculations in Figure 2.

a (m)	e (m)	r (m)	h_1 (m)	h_2 (m)	R_{S1} (m)	R_{S2} (m)
0.1	0.005	0.04	0.01	0.03	0.046	0.043

In order to understand the influence mechanisms clearly, the simplified model of stubbed-on LRPC DPS is proposed, as shown in Figure 3a. In the model, the upper and lower plates were reduced to thin plates, and the resonator unit was reduced to spring and mass; the surrounded soft shell was reduced to surrounded springs. Here, four springs were taken into consideration. FEM was also used to calculate the band structures of the simplified models [19]. Here, the elasticity modulus, Poisson's ratio, and density of the base plates are represented by E , μ , and ρ , respectively. The spring stiffness, mass, and one additional spring stiffness are denoted by k_R , m_R , and k_A . Moreover, the thickness of base plates is h and the lattice constant is a . The distance between the additional spring and spring in the resonator is $a/4$.

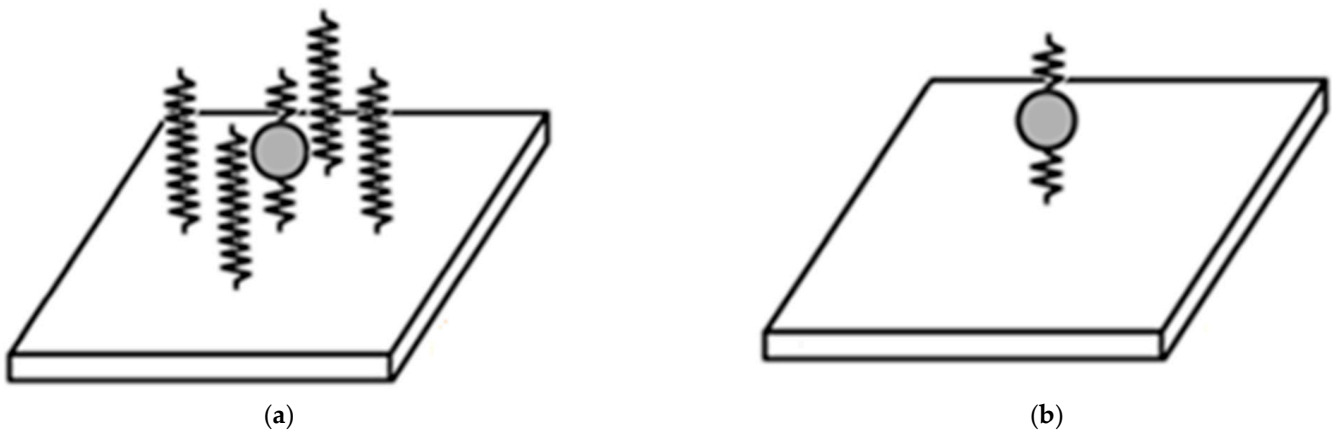


Figure 3. The unit cells of simplified models (the upper plate is ignored) with (a) four and (b) zero springs surrounded.

Figure 4a,b show the band structures of simplified models of stubbed-on LRPC DPSs with four and zero additional springs surrounded, respectively. All the materials' parameters and geometric parameters used in calculations are shown in Tables 3 and 4, respectively. As shown in the figure, the additional springs only affect the bands corresponding to symmetric vibration mode but have no effect on the bands corresponding to antisymmetric vibration mode, which is the same as the phenomenon of stubbed-on LRPC DPSs displayed in Figure 3. Furthermore, the springs added also make the bands corresponding to symmetric vibration mode move up.

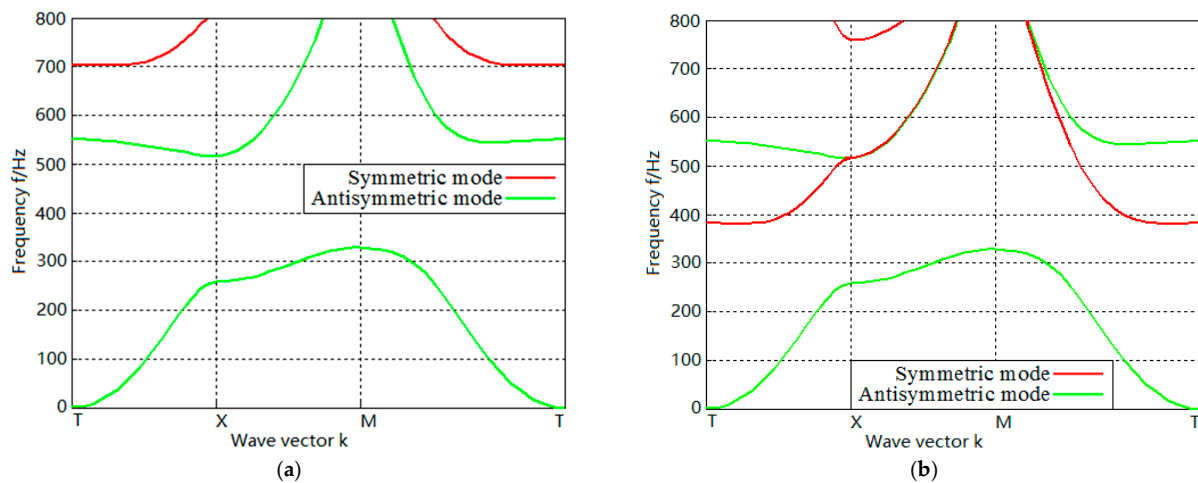


Figure 4. Band structures of simplified models of stubbed-on LRPC DPSs with (a) four and (b) zero springs surrounded.

Table 3. Materials’ parameters used in calculations in Figure 4.

$E(\text{GPa})$	μ	$\rho(\text{kg}\cdot\text{m}^{-3})$	$k_R(\text{Nm}^{-1})$	$m_R(\text{kg})$	$k_A(\text{Nm}^{-1})$
77.6	0.35	2730	4×10^5	0.1	1×10^5

Table 4. Geometric parameters used in calculations in Figure 4.

$h(\text{m})$	$a(\text{m})$	$R_s(\text{m})$
0.002	0.1	4×10^{-6}

The “base-spring-mass” simplified model of vibration modes has been widely used to help understand the formation mechanisms of the band gap [12,18,20]. Here, the model was also applied, as shown in Figure 5. For mode B_8 labeled in Figure 2b, the corresponding displacement field is shown in Figure 6, which was also obtained by using FEM [18]. As shown in the figure, the middle Pb layer of the pillar remains stationary, which can be equivalent to base m shown in Figure 5. In addition, the rubber layer of pillar and plates can be equivalent to spring k and mass M . Hence, it can be understood that surrounding soft shell or adding springs makes the equivalent spring increase, which increases the frequency corresponding to B_8 and leads the band to rise. However, for antisymmetric vibration mode, the two plates vibrate in the same phase, which leads the surrounding soft shell or adding springs to hardly work.

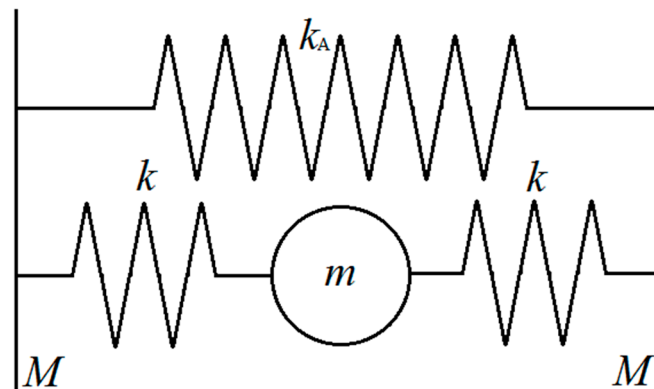


Figure 5. The “base-spring-mass” simplified model of vibration modes.

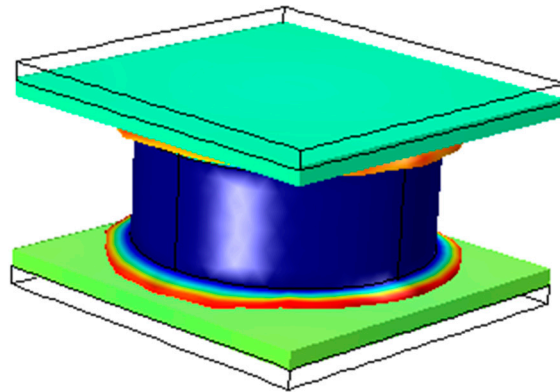


Figure 6. The displacement field corresponding to vibration mode B₈.

3.2. Influences of Soft Shell Parameters on Band Gap

As known from the above section, the additional soft shell plays an active role in widening the band gap but does not affect the starting frequency. Here, the elasticity modulus, Poisson's ratio, and density of soft shell were picked to investigate the influences of the materials' parameters on the band gap. All the parameters except for the materials' parameters of the soft shell are shown in Tables 1 and 2, and the materials' parameters of the soft shell were presupposed to be elasticity modulus $E_a = 1.175 \times 10^5 \text{ N/m}^2$, Poisson's ratio $\mu_a = 0.469$, and density $\rho_a = 0 \text{ kg/m}^3$, respectively. What should be noted is that all the others are the default if one was chosen as the influencing parameter.

Figure 7 shows the band structures of LRPC DPSs if the densities of soft shell are $\rho_a = 10 \text{ kg/m}^3$, $\rho_a = 20 \text{ kg/m}^3$ and $\rho_a = 30 \text{ kg/m}^3$, respectively. By comparing Figure 7 with Figure 2a, the density of soft shell has little effect on bands corresponding to B₁–B₉, but has obvious influences on some flat bands, which makes the corresponding frequencies of flat bands reduce and leads the flat bands to decline to the frequency region under the band corresponding to B₈. It can be understood that the increase of soft shell density makes the equivalent mass of flat band modes increase, which leads the corresponding frequencies to reduce. In fact, the effects of flat bands on band gap can be ignored if only a few flat bands are located in the frequency range of the original band gap.

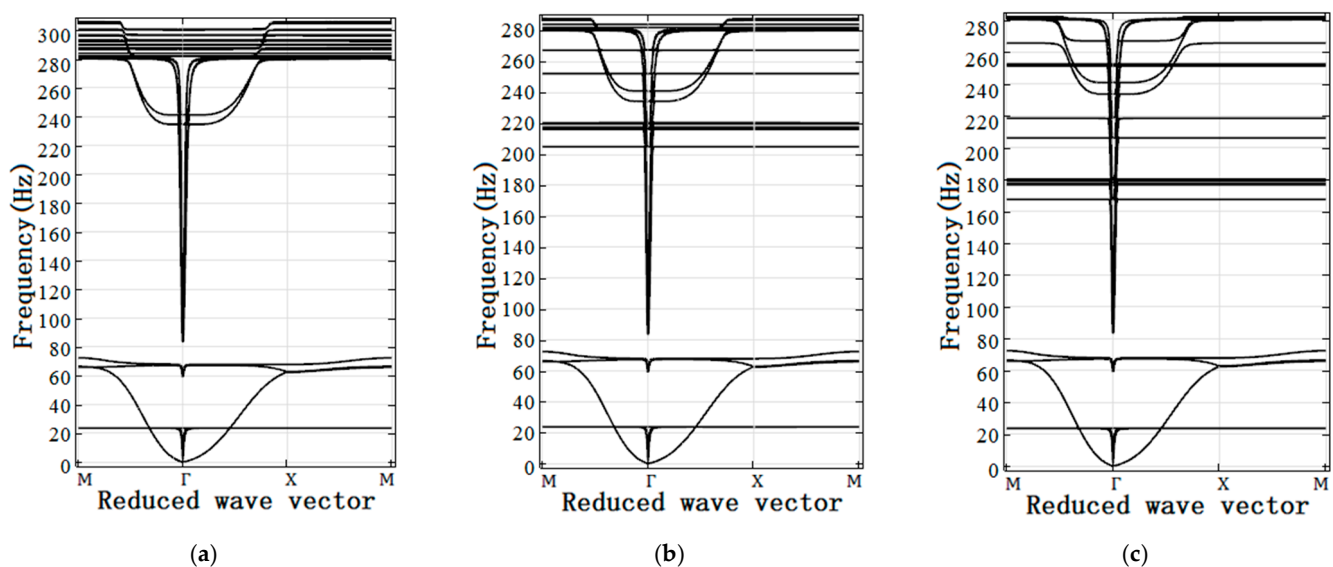


Figure 7. Band structures of LRPC DPSs if the densities of soft shell are (a) $\rho_a = 10 \text{ kg/m}^3$, (b) $\rho_a = 20 \text{ kg/m}^3$ and (c) $\rho_a = 30 \text{ kg/m}^3$, respectively.

Figure 8 displays the band structure of LRPC DPS if the Poisson's ratio of soft shell is $\mu_a = 0.2$. By comparing Figure 8 with Figure 2a, the band structures are the same; that is, Poisson's ratio of the soft shell has no effect on the band structure. Because Poisson's ratio determines shear modulus if elasticity modulus is given, it illustrates that adding a soft shell only affects the bands corresponding to flexural vibration mode, but not longitudinal vibration mode.

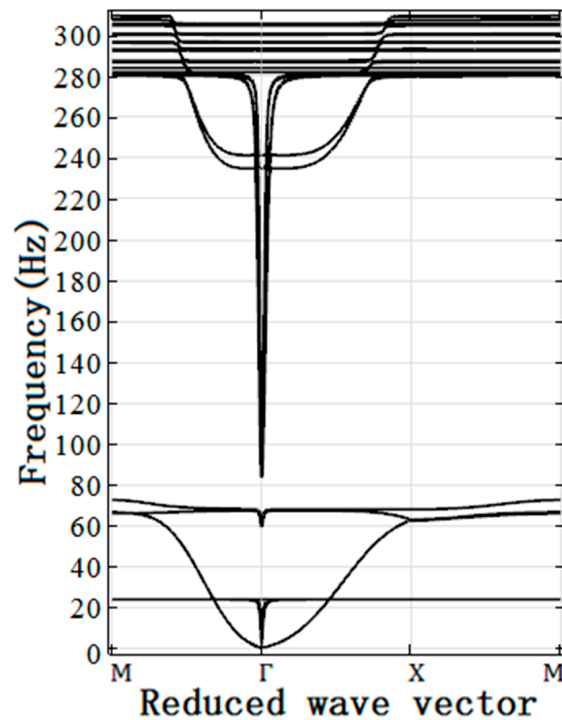


Figure 8. Band structure of LRPC DPS if the Poisson's ratio of soft shell is $\mu_a = 0.2$.

The band structures of LRPC DPSs are shown in Figure 9 if the elasticity moduli of the soft shell are $E_a = 1 \times 10^6 \text{ N/m}^2$ and $E_a = 2 \times 10^6 \text{ N/m}^2$, respectively. By comparing Figure 9 with Figure 2a, the elasticity modulus of the soft shell has no apparent effect on bands corresponding to B_1 – B_7 and B_9 , but has obvious influence on bands corresponding to B_8 . It can be attributed to that for modes B_1 – B_3 and antisymmetric vibration mode B_9 , the upper and lower plates remain relatively static [18]; but for longitudinal vibration modes B_4 – B_7 , the conclusion has been obtained from the previous analysis that adding a soft shell only affects the bands corresponding to the flexural vibration mode.

In order to further illustrate the influence rule of elasticity modulus, the influences of elasticity moduli on soft shell E_a on critical frequencies f_3 , f_8 , f_9 , and band gap width f_w are displayed in Figure 10. Here, f_3 , f_8 , and f_9 are the frequencies corresponding to vibration modes B_3 , B_8 , and B_9 , respectively. As shown in the figure, E_a has no effect on f_3 and f_9 indeed. However, with the increase of E_a , f_8 increases, which is on account of that the restrain of soft shell on the band corresponding to symmetric vibration mode strengthens with the increase of E_a . In addition, $f_8 > f_9$ if $E_a > 5 \times 10^5 \text{ N/m}^2$, the band gap width f_w is determined by the constant starting frequency f_3 and constant ending frequency f_9 ; $f_8 < f_9$ if $E_a < 5 \times 10^5 \text{ N/m}^2$, the band gap width f_w is determined by the constant starting frequency f_3 and increasing ending frequency f_8 . Hence, the starting frequency keeps still, and the band gap width increases first and then keeps constant with the increase of elasticity modulus.

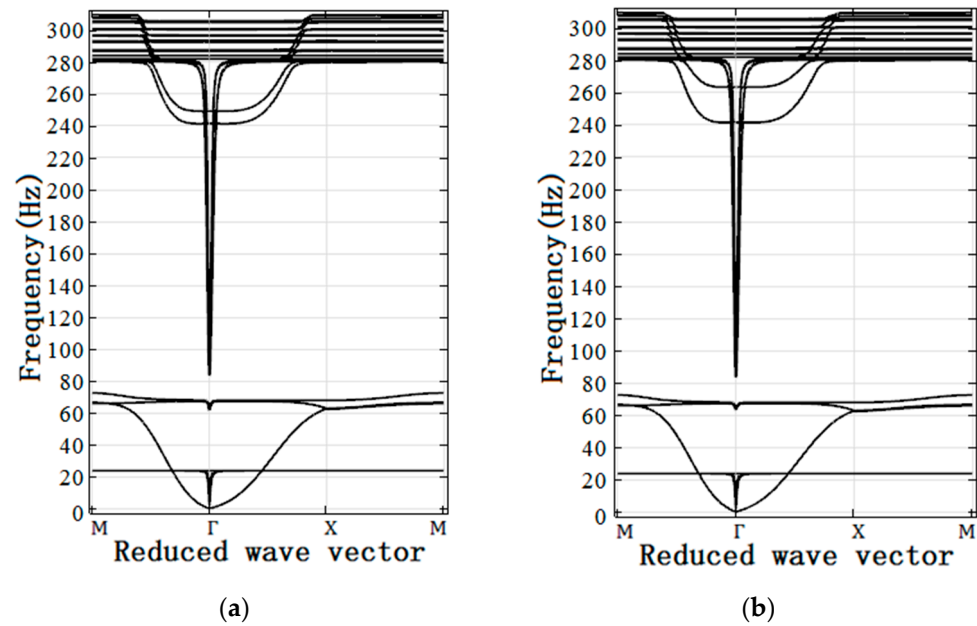


Figure 9. Band structures of LRPC DPSs if the elasticity moduli of the soft shell are (a) $E_a = 1 \times 10^6$ N/m² and (b) $E_a = 2 \times 10^6$ N/m², respectively.

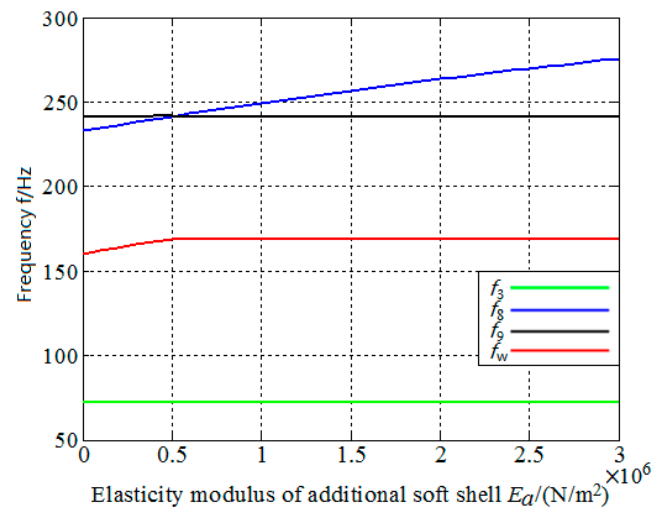


Figure 10. The influences of elasticity moduli of soft shell E_a on critical frequencies f_3 , f_8 , f_9 , and band gap width f_w .

4. Conclusions

In this paper, the stubbed-on LRPC DPS with a soft shell surrounded and simplified model with additional springs surrounded are proposed based on the stubbed-on LRPC DPS made of a two-dimensional periodic array of a two-component cylindrical LR pillar connected between the upper and lower plates. Further, the influence mechanisms and rules of added soft shell on band gap are investigated by using FEM. The main conclusions are as follows:

A complete band gap with a low starting frequency and wide band width is opened if the excitation and response points are picked on different sides of DPS. Comparing the band structures of DPSs with and without a soft shell surrounded and comparing the band structures of simplified models with and without additional springs surrounded, what can be concluded is that the soft shell only affects the bands corresponding to symmetric

vibration mode and makes the bands shift up, which plays an active role in widening the band gap.

The density of soft shell has little effect on bands formed in the original band gap, but makes some flat bands move down to the frequency region of band gap. In fact, the effects of flat bands on the band gap can be ignored if only a few flat bands located in the frequency range of the original band gap. The Poisson's ratio of soft shell has no effect on band structure, which illustrates that adding a soft shell only affects the bands corresponding to flexural vibration mode, but not longitudinal vibration mode. The elasticity modulus of the soft shell only influences the bands corresponding to symmetric flexural vibration mode, and the starting frequency keeps still, and the band gap width increases first and then keeps constant with the increase of elasticity modulus.

Author Contributions: Conceptualization, Y.X.; formal analysis, Y.X.; investigation, Y.X., M.C., D.Q. and Z.S.; data curation, Y.X.; writing—original draft preparation, Y.X. and M.C.; writing—review and editing, Y.X., D.Q. and Z.S.; funding acquisition, D.Q. All authors have read and agreed to the published version of the manuscript.

Funding: This research was supported by the National Natural Science Foundation of China (No. 11847009).

Conflicts of Interest: The authors declare no conflict of interest.

References

1. Heo, J.W.; Chung, J.; Choi, K. Dynamic time responses of a flexible spinning disk misaligned with the axis of rotation. *J. Sound Vib.* **2003**, *262*, 25–44. [[CrossRef](#)]
2. Rossetti, D.J.; Norris, M.A. A comparison of actuation and sensing techniques for aircraft cabin noise control. *Noise Control Eng. J.* **1996**, *44*, 53–58. [[CrossRef](#)]
3. Valoor, M.T.; Chandrashekhara, K.; Agarwal, S. Self-adaptive vibration control of smart composite beams using recurrent neural architecture. *Int. J. Solids Struct.* **2001**, *38*, 7857–7874. [[CrossRef](#)]
4. Jung, J.-W.; Lee, S.-H.; Lee, G.-H.; Hong, J.-P.; Lee, D.-H.; Kim, K.-N. Reduction Design of Vibration and Noise in IPMSM Type Integrated Starter and Generator for HEV. *IEEE Trans. Magn.* **2010**, *46*, 2454–2457. [[CrossRef](#)]
5. Pietrzko, S.J.; Mao, Q. New results in active and passive control of sound transmission through double wall structures. *Aerosp. Sci. Technol.* **2008**, *12*, 42–53. [[CrossRef](#)]
6. Thongchom, C.; Saffari, P.R.; Refahati, N.; Saffari, P.R.; Pourbashash, H.; Sirimontree, S.; Keawsawasvong, S. An analytical study of sound transmission loss of functionally graded sandwich cylindrical nanoshell integrated with piezoelectric layers. *Sci. Rep.* **2022**, *12*, 3048. [[CrossRef](#)]
7. Thongchom, C.; Jearsiripongkul, T.; Refahati, N.; Saffari, P.R.; Saffari, P.R.; Sirimontree, S.; Keawsawasvong, S. Sound Transmission Loss of a Honeycomb Sandwich Cylindrical Shell with Functionally Graded Porous Layers. *Buildings* **2022**, *12*, 151. [[CrossRef](#)]
8. Sigalas, M.M.; Economou, E.N. Elastic and acoustic wave band structure. *J. Sound Vib.* **1992**, *158*, 377–382. [[CrossRef](#)]
9. Liu, Z.; Zhang, X.; Mao, Y.; Zhu, Y.Y.; Yang, Z.; Chan, C.T.; Sheng, P. Locally Resonant Sonic Materials. *Science* **2000**, *289*, 1734–1736. [[CrossRef](#)]
10. Zhang, X.; Liu, Z.; Liu, Y. Elastic wave band gaps for three-dimensional phononic crystals with two structural units. *Phys. Lett. A* **2003**, *313*, 455–460. [[CrossRef](#)]
11. Ho, K.M.; Cheng, C.K.; Yang, Z.; Zhang, X.X.; Sheng, P. Broadband locally resonant sonic shields. *Appl. Phys. Lett.* **2003**, *83*, 5566–5568. [[CrossRef](#)]
12. Oudich, M.; Li, Y.; Assouar, B.; Hou, Z. A sonic band gap based on the locally resonant phononic plates with stubs. *New J. Phys.* **2010**, *12*. [[CrossRef](#)]
13. Badreddine Assouar, M.; Oudich, M. Enlargement of a locally resonant sonic band gap by using double-sides stubbed phononic plates. *Appl. Phys. Lett.* **2012**, *100*, 123506. [[CrossRef](#)]
14. Hsu, J.C. Local resonances-induced low-frequency band gaps in two-dimensional phononic crystal slabs with periodic stepped resonators. *J. Phys. D Appl. Phys.* **2011**, *44*, 055401. [[CrossRef](#)]
15. Xiao, Y.; Wen, J.; Wen, X. Flexural wave band gaps in locally resonant thin plates with periodically attached spring-mass resonators. *J. Phys. D Appl. Phys.* **2012**, *45*, 195401. [[CrossRef](#)]
16. Ruan, Y.; Liang, X.; Hua, X.; Zhang, C.; Xia, H.; Li, C. Isolating low-frequency vibration from power systems on a ship using spiral phononic crystals. *Ocean Eng.* **2021**, *225*, 108804. [[CrossRef](#)]
17. Xiao, W.; Zeng, G.W.; Cheng, Y.S. Flexural vibration band gaps in a thin plate containing a periodic array of hemmed discs. *Appl. Acoust.* **2008**, *69*, 255–261. [[CrossRef](#)]
18. Qian, D.; Shi, Z. Bandgap properties in locally resonant phononic crystal double panel structures with periodically attached pillars. *J. Theor. Appl. Mech.* **2017**, *55*, 1167–1179. [[CrossRef](#)]

19. Qian, D.; Shi, Z. Bandgap properties in locally resonant phononic crystal double panel structures with periodically attached spring-mass resonators. *Phys. Lett. A* **2016**, *380*, 3319–3325. [[CrossRef](#)]
20. Wang, Y.F.; Wang, Y.S.; Su, X.X. Large bandgaps of two-dimensional phononic crystals with cross-like holes. *J. Appl. Phys.* **2011**, *110*, 2059. [[CrossRef](#)]